ACS Photonics
Article
pubs.acs.org/journal/apchd5

M-Plane GaN/InAlN Multiple Quantum Wells in Core–Shell Wire Structure for UV Emission

Christophe Durand,*[†] Catherine Bougerol,[‡] Jean-François Carlin,[§] Georg Rossbach,[§] Florian Godel,[†] Joël Eymery,[†] Pierre-Henri Jouneau,[||] Anna Mukhtarova,[†] Raphaël Butté,[§] and Nicolas Grandjean[§]

[†]Equipe mixte CEA-CNRS "Nanophysique et Semiconducteurs", SP2M, UMR-E CEA/UJF-Grenoble 1, INAC, Grenoble, 38054, France

[‡]Equipe mixte CEA-CNRS "Nanophysique et semiconducteurs", Institut Néel-CNRS, 25 rue des Martyrs, 38042 Grenoble Cedex 9, France

[§]Institute of Condensed Matter Physics (ICMP), Ecole Polytechnique Fédérale de Lausanne (EPFL), CH-1015, Lausanne, Switzerland

[||]LEMMA, SP2M, UMR-E CEA/UJF-Grenoble 1, INAC, Grenoble, 38054, France

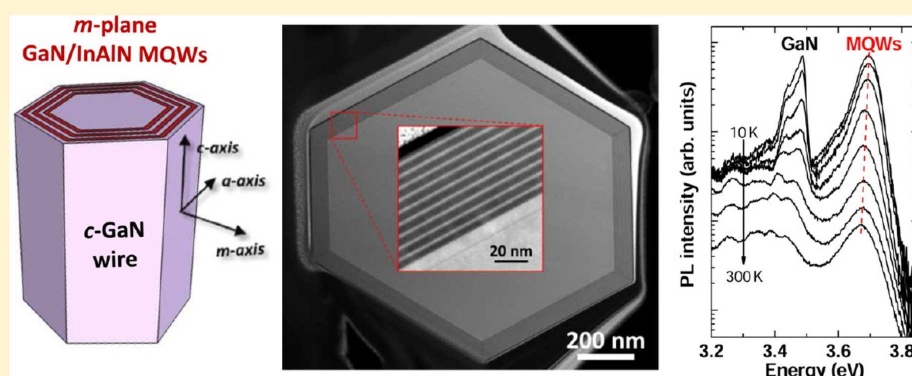

ABSTRACT: We report on the epitaxial growth of high-quality core–shell nonpolar *m*-plane GaN/InAlN multiple quantum wells (MQWs) on the sidewall facets of *c*-oriented hexagonal GaN wires. Pseudomorphic growth without generation of threading dislocations has been established for planar GaN/InAlN (In = 15%) MQWs grown on *m*-GaN substrates, although *m*-plane InAlN epilayers cannot be grown perfectly lattice-matched to GaN along the two in-plane directions. Calculations based on elasticity theory indicate that the significant amount of strain oriented along the *c*-axis is the likely factor favoring the formation of cracks along this direction. For the core–shell wire geometry, such cracks are not observed, leading to high structural quality MQWs. A significant UV emission centered around 3.7 eV at room temperature with a strong polarization perpendicular to the wire axis is observed for those core–shell wires, which is consistent with $k\cdot p$ method calculations, proving the absence of quantum confined Stark effect on nonpolar *m*-plane surfaces. These excellent optical features reported in the UV spectral range are attributed to the defect-free nature of the GaN/InAlN MQWs, thereby opening promising opportunities for the realization of UV light emitters.

KEYWORDS: *GaN, InAlN, m-plane nonpolar growths, nitride wires, core–shell heterostructures, multiple quantum wells, UV emission*

During the past decade, the development of nanowires (NWs) has made significant progress, making them a serious alternative as functional building blocks to design new photonic or electronic devices.[1,2] NW growth is currently well-controlled for III–V semiconductor materials as exemplified by the achievement of vertical NW ordered arrays,[3] doping modulation,[4] and complex axial/radial heterostructures.[5] In the case of III-nitrides, NWs have gained a lot of attention with the pioneering demonstrations of single-NW devices such as high electron mobility transistors (HEMTs) built from GaN/AlN/AlGaN heterostructures[6] or light emitting diodes (LEDs),[7] lasers,[8] and photovoltaic cells,[9] using InGaN/GaN multiple quantum wells (MQWs). Significant efforts are currently being pursued to achieve effective devices based on nitride NWs, especially to fabricate LEDs.[10] It has been emphasized that the wire geometry offers key advantages to further improve the performance of nitride devices compared to the standard planar technology. First, the growth of nanostructures, such as NWs, can be performed on various low-cost substrates such as Si[11] or glass[12] to fabricate LED devices. Second, the sidewalls of *c*-plane oriented GaN wires can be considered as a *m*-plane GaN template for MQW growth, as already reported for core–shell InGaN/GaN MQW

Received: September 10, 2013
Published: November 12, 2013

ACS Publications © 2013 American Chemical Society

LEDs showing a strong blue electroluminescence at room temperature and the absence of quantum confined Stark effect (QCSE), in agreement with their nonpolar orientation.[13] Third, a significant reduction in the dislocation density is expected in the active region that should drastically improve the internal quantum efficiency (IQE). For instance, an IQE above 50% is theoretically predicted for dislocation densities less than 10^9 cm^{-2} in the case of AlGaN-based MQWs for UV emission.[14] For core−shell heterostructures, the threading dislocations (TDs) formed at the wire−substrate interface do not affect the shell active region and efficient UV emission can be envisioned. This latter point is one of the important issues to address the limited efficiency of the current planar technology for the development of UV LEDs.[15,16] Up to now, only the growth of core−shell GaN/AlN MQWs has been explored on triangular catalyzed GaN wires showing the proof of concept of the wire technology for UV emission.[17]

Within the same decade, the InAlN nitride alloy has attracted a lot of attention due to the possibility to realize in-plane lattice-matched (LM) heterostructures with *c*-GaN for an indium content close to 17−18%.[18] Though the epitaxy of InAlN is challenging, notable progress has been made in the growth of high-quality thin InAlN layers and GaN/InAlN multilayers on *c*- plane GaN templates, making such GaN/InAlN heterostructures an alternative candidate for next-generation III-nitride devices.[19,20] For instance, HEMTs based on a strain-free InAlN thin barrier layer grown on top of GaN have been successfully demonstrated.[21] InAlN has also been efficiently used as an electron blocking layer.[22] In addition, defect-free LM GaN/InAlN multilayers have been employed as distributed Bragg mirrors,[23−25] near-infrared, inter-sub-band superlattices showing absorption or UV emission.[26] Those MQWs could also potentially compete with GaN/AlGaN MQWs exhibiting a higher brightness of UV light at room temperature.[20] InAlN-based heterostructures have to therefore be considered as an alternative active region to realize efficient near-UV light emitters. LM InAlN-based heterostructures grown along the conventional polar *c*-axis direction are known to present a strong built-in electric field of pure spontaneous origin, which amounts to 3.6 MV/cm in single *c*-plane GaN/InAlN quantum wells (QWs).[19,26,27] The resulting built-in electric field causes the undesirable QCSE in the case of quantum wells, which is known to be responsible for a significant red-shift in the emission energy and a decreased radiative efficiency of LEDs. InAlN growth along nonpolar directions has been much less studied than along the polar one, whereas the absence of polarization mismatch should lead to higher exciton oscillator strength and higher light emission efficiency[28] making nonpolar orientation of high interest for microcavities[29] or UV light emitters. However, in the case of *m*-plane nonpolar growths, the plane perpendicular to the growth axis is defined by two independent lattice parameters, namely, "*a*" and "*c*" of the hexagonal cell. As a consequence, in-plane lattice matching cannot be simultaneously obtained along both directions, resulting in anisotropic in-plane strain. This is markedly different from the case of *c*-plane growth for which perfect lattice matching can be achieved along the *a*-axis for an In composition close to 17%.[18,19] The growth of an *a*-plane (11−20) InAlN layer on *a*-GaN/*r*-sapphire has been recently reported showing anisotropic structural and optical properties for films with 19% of indium.[30] Also, high-quality, *m*-plane (1−100) InAlN growth on ZnO substrates has been performed using a room-temperature epitaxial growth technique for In composition below 50%.[31] These examples prove that the epitaxy of nonpolar InAlN layers nearly lattice matched with GaN can be achieved, thereby motivating the extension to nonpolar GaN/InAlN MQWs.

In this work, we investigate the growth of *m*-plane GaN/InAlN MQWs on planar *m*-GaN substrates and *m*-plane sidewall facets of *c*-oriented hexagonal GaN wires, as depicted in Figure 1. In the case of planar growths, the epitaxy and the in-plane strain anisotropy will be discussed by combining X-ray and microscopy experiments and will be related to elasticity theory calculations. A significant strain along the *c*-axis is clearly identified causing cracks along this direction. For the wire geometry, the growth of core−shell MQWs on GaN wire sidewalls is performed without the formation of such cracks. Defect-free GaN/InAlN MQWs in the core−shell wire geometry exhibit strong photoluminescence around 3.7 eV up to room temperature, contrary to equivalent *m*-plane planar structures, proving the interest of the wire-based design for UV light emitting devices.

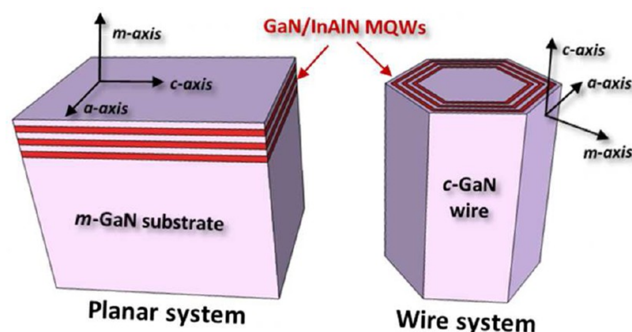

Figure 1. Schematic diagram of the two different geometries considered to grow nonpolar *m*-plane GaN/InAlN MQWs: (1) planar growth on an *m*-GaN substrate and (2) core−shell growth on the sidewall facets of *c*-oriented GaN wires.

GaN wires having lateral {1−100} *m*-plane facets and a length about 30 μm are grown in a metal−organic vapor-phase epitaxy (MOVPE) close-coupled showerhead reactor on *c*-plane sapphire substrates. The wires are obtained by combining *in situ* pretreatment favoring the formation of an N-polar GaN hexagonal seed, a silane flux, and a low V/III ratio in order to promote the vertical growth (see details in refs 32 and 33). After a certain length (∼20 μm), the silane injection is stopped to grow an unintentionally doped GaN section (∼10 μm) at the top of the wires. Then in an AIXTRON 200/4 RF-S MOVPE system, nine GaN/InAlN MQWs are grown after a preannealing at 1000 °C under hydrogen during 5 min to clean the wire surfaces (no degradation of the wire shape is observed after the annealing step). The growth of the core−shell MQW structure is performed at 835 °C under ammonia flux using both trimethyl-indium and trimethyl-aluminum for InAlN growth and trimethyl-gallium for GaN growth. The nominal In composition of InAlN barriers is fixed at 17−18% and the nominal GaN and AlInN layer thicknesses are 2 and 5 nm, respectively. Electron microscopy analysis has been carried out either in transmission (TEM) or scanning- transmission (STEM) mode on Jeol 3010 and probe-corrected FEI-Titan microscopes operated at 300 kV. Slices of the wires, either parallel or perpendicular to the growth axis, have been prepared by focused ion beam (FIB). For planar growths, samples have been prepared in cross sections by mechanical polishing and

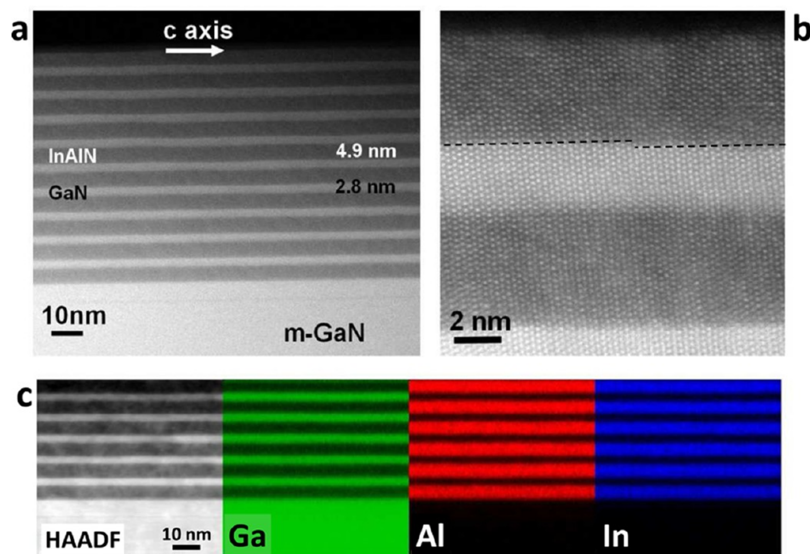

Figure 2. TEM characterization of planar *m*-plane GaN/InAlN MQWs. (a) STEM-HAADF image of MQWs taken along the [11−20] zone axis. (b) Enlarged image of single GaN wells. The dashed line indicates the atomic steps at the GaN/InAlN interface. (c) EDX chemical characterization showing HAADF image and the corresponding Ga, Al, and In mappings in green, red, and blue, respectively.

subsequent ion-milling (Gatan PIPS operated at 3 keV). Local Ga, In, and Al compositions have been measured by energy dispersive X-ray spectroscopy (EDX). This has been done on an FEI Osiris TEM operated at 200 kV, and fitted with a high brightness gun with four windowless silicon drift detectors (SDD) combined symmetrically around the objective lens. This configuration offers a large X-ray collection angle (∼0.9 sr) that permits the efficient acquisition of EDX spectral images. Quantitative elemental maps are then calculated using the Cliff-Lorimer ratio technique. High resolution X-ray diffraction (HRXRD) reciprocal space mappings have been used to get access to the strain state of planar structures at the macroscopic scale. We used a standard setup equipped with a beam concentrator, a Ge (220) four-bounce monochromator and a Ge analyzer in front of the detector. Photoluminescence (PL) spectroscopy at 5 K using a frequency-doubled continuous wave Ar^+ laser excitation source emitting at 244 nm has been carried out to study the optical properties of GaN/InAlN MQWs grown on planar GaN substrates or wire sidewalls. Microphotoluminescence (micro-PL) and cathodoluminescence (CL) experiments have also been performed on dispersed wires to gain insights on the local light emission of single wires. For CL mappings, the electron beam voltage and current were set to 20 kV and 1 nA, respectively. For micro-PL measurements, the laser beam was focused by means of a UV microscope objective with a numerical aperture of 0.55. The corresponding spot size amounts to ∼5 μm for the polarization-resolved measurements, whereas proper shaping of the laser beam and guiding through a UV microscope stand allowed reaching a nearly diffraction-limited spot size of ∼0.5 μm for the temperature-dependent micro-PL measurements. Polarization-selection was obtained using a Glan polarizer and its response has been calibrated by white light reflection under normal incidence. The PL and CL collected signals were sent to a monochromator combined with a liquid-nitrogen cooled UV-enhanced charge-coupled device providing a spectral resolution of about 2 meV.

To get structural and optical features of such *m*-plane growths, nonpolar GaN/InAlN MQWs directly grown on *m*-plane GaN substrates have been first investigated with a specific focus on the strain state of these heterostructures. The STEM-high angle annular dark field (HAADF) image (Figure 2a) taken along the [11−20] zone axis shows the *m*-plane epitaxy of the MQW structure consisting of 2.8 nm GaN layers (bright contrast) separated by 4.9 nm InAlN layers (dark contrast). No dislocations or stacking faults are observed, which is notably different from the case of *m*-plane AlN/GaN heterostructures.[34] However, cracks are visible along the *c*-axis in the [10−10] zone axis, as mentioned afterward. The interfaces do not present exactly the same sharpness (Figure 2b): along the growth direction, the top interface of the InAlN layers is relatively wavy, whereas the top surface of the GaN layers appears flatter with atomic steps between terraces (terrace length about 10 nm). Regarding the InAlN layer, we notice the rather homogeneous distribution of bright spots (related to In atoms) among dark ones (Al atoms), which indicates that no marked In clustering occurs at this scale (Figure 2b). This is supported by chemical mappings obtained by EDX. Figure 2c shows a sharp interface composition, and mappings indicate a homogeneous composition in Al and In within the InAlN barrier layers corresponding to an In content of 15% (± 2%).

High resolution (HR) STEM images taken along the [0001] and [11−20] zone axes have been analyzed by geometrical phase analysis (GPA),[35] in order to obtain lattice parameter mappings along the three main directions, namely, *a*- and *c*-maps for the in-plane parameters and *m*-map for the parameter along the growth axis. GaN was taken as the reference region. The results are given in Figure 3a−d. Both *a*- and *c*-maps present random fluctuations within the error bars (Figure 3b,c), meaning that InAlN and GaN layers adopt the same in-plane lattice parameters. On the contrary, the InAlN layers exhibit a lattice spacing 1.5% smaller than the GaN one along the growth direction (*m*-mapping in Figure 3d). As no difference was observed on GPA maps between GaN layers and the GaN substrate (not shown here), the values of the lattice parameters of GaN within the layers are those of relaxed GaN, that is, a = 0.3189 nm and c = 0.5185 nm.[36] The pseudomorphic growth of the planar MQWs has also been verified by means of HRXRD

dx.doi.org/10.1021/ph400031x | ACS Photonics 2014, 1, 38−46

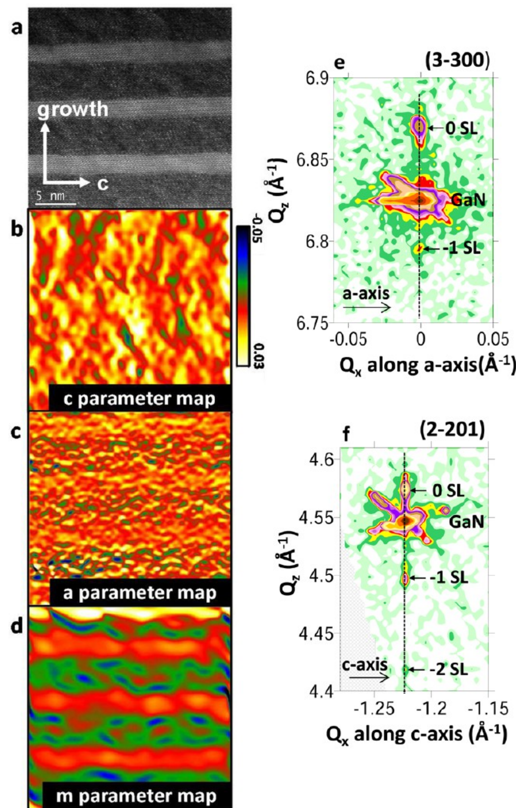

Figure 3. Lattice parameter study of planar *m*-plane GaN/InAlN MQWs. GPA analyses based on STEM images taken along the [0001] and [11−20] zone axes: (a) STEM image with g = [11−20], (b, c) mapping of in-plane parameters, i.e., *c*- and *a*-lattice parameter, respectively, (d) mapping of the out-of plane *m*-lattice parameter. (e, f) Reciprocal space maps taken around the asymmetric (3−300) and (2−201) reflections for the azimuthal directions corresponding to the two in-plane directions (i.e., the *a*- and *c*-axis). The broadening of the XRD peaks is related to the low-resolution limitation of the experimental XRD setup.

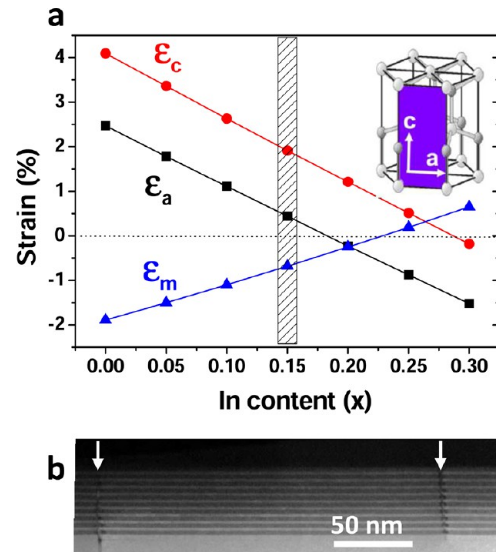

Figure 4. (a) Calculation of the strain components ε_a, ε_c, and ε_m as a function of In content for *m*-plane InAlN growth on GaN, indicating that the residual strain is always present for the *m*-plane orientation whatever the In content. (b) TEM image taken along the [11−20] zone axis showing cracks along the *c*-axis direction for which the strain is the most significant for InAlN layers with an In content equal to 15%.

reciprocal space mappings. The mappings are performed around the $(3\ \bar{3}\ 0\ 0)$ and $(2\ \bar{2}\ 0\ 1)$ Bragg peaks for the azimuthal directions corresponding to the *a*- and *c*-axis (called Q_x-axis) perpendicular to the *m*-plane direction (Figure 3e,f). For these two reflections, Q_z corresponds to the *m*-direction and to the $[2\ \bar{2}\ 0\ 1]$-direction, respectively. Figure 3e,f shows that the MQW superlattice (SL) peaks are aligned along the Q_z direction, confirming the absence of in-plane strain relaxation (i.e., coherent growth).[37] This X-ray diffraction investigation unambiguously supports the local-scale STEM-HAADF image analysis reported before.

In the framework of elasticity theory, we have determined the strain components ε_a, ε_c, and ε_m to estimate the strain state of those *m*-plane samples as a function of In content (Figure 4a). The elastic constants of AlN and InN (taken from ref 38) are linearly interpolated as a function of composition, as well as the lattice parameters of the $In_xAl_{1-x}N$ alloy.[39] The strain components are then given by

$$\varepsilon_a = \frac{a_x}{a_{ox}} - 1 \tag{1}$$

$$\varepsilon_c = \frac{c_x}{c_{ox}} - 1 \tag{2}$$

$$\varepsilon_m = -\frac{C_{12}}{C_{11}}\varepsilon_a - \frac{C_{13}}{C_{11}}\varepsilon_c \tag{3}$$

where a_{0x} and c_{0x} are the lattice parameters of the relaxed $In_xAl_{1-x}N$ alloy, a_x and c_x are those of the $In_xAl_{1-x}N$ layer, strained to $a_x = a_{GaN}$ and $c_x = c_{GaN}$, and C_{ij} are the elastic constants (i,j = 1, 2, 3).

From Figure 4a, ε_a and ε_c cannot be canceled for the same x value ($\varepsilon_a = 0$ for x = 18%, while $\varepsilon_c = 0$ for x = 29%) due to the in-plane anisotropy inherent to *m*-plane heterostructures. Therefore, a residual strain is necessarily present whatever the In content, contrary to *c*-plane GaN/InAlN heterostructures for which it is possible to find an In composition corresponding to a perfect in-plane lattice matching.

The In content can be estimated from X-ray diffraction, HR-STEM measurements and elasticity theory. The d_{110}^{GaN} and average SL d_{110}^{SL} spacings have been obtained from X-ray $\theta - 2\theta$ scans. Assuming that the average SL d_{110}^{SL} interplanar distance is related to d_{110}^{GaN} and d_{110}^{InAlN} by the following expression:

$$n^{GaN}\cdot d_{110}^{GaN} + n^{InAlN}\cdot d_{110}^{InAlN} = (n^{GaN} + n^{InAlN})\cdot d_{110}^{SL} \tag{4}$$

where n^{GaN} and n^{InAlN} are the number of GaN and InAlN monolayers and $t^{GaN} = n^{GaN}\cdot d_{110}^{GaN}$ and $t^{InAlN} = n^{InAlN}\cdot d_{110}^{InAlN}$ are the thicknesses of the GaN and InAlN layers measured on HR-STEM images (Figure 2a); we find that d_{110}^{InAlN} = 0.273 nm. From elasticity theory, we have then deduced that the In concentration in the samples was equal to 15%, in agreement with the EDX results. The *m*-plane surface is known to incorporate less In atoms than the standard *c*-plane surface for InGaN-based MQWs.[40,41] We observe the same behavior in the case of InAlN, because the In content is measured around 15% for a nominal value fixed at 17−18%. Knowing this composition, we can extract from Figure 4a the strain components along *a*, *c*, and *m*, which are equal to 0.57, 2.05, and −0.77%, respectively. The large value for ε_c (2.05%) is

consistent with the TEM observation of cracks along this direction, as shown in Figure 4b.

The optical properties of planar *m*-plane GaN/InAlN MQWs have been measured by PL at 5 K. Figure 5 shows a PL spectrum that clearly exhibits an intense contribution assigned to the near-band edge (NBE) emission originating from the bulk *m*-GaN substrate. The NBE emission is composed of the donor bound exciton recombination (D^0X) peak at 3.47 eV and the D^0X two electron satellite (TES) peak at 3.45 eV.[42] We also observe the first two longitudinal optical (LO) phonon replicas of the D^0X emission at 3.38 and 3.29 eV, respectively, labeled 1LO and 2LO in Figure 5. The signature of MQW emission is weakly visible on the high-energy side of the PL spectrum. This contribution is centered at ∼3.55 eV with a full width at half-maximum (fwhm) being equal to 110 meV. The emission intensity is extremely low and the line width is larger compared to that measured on *c*-plane InAlN- based nitride MQWs (65 meV) reported in ref 26. The weak PL signal from those MQWs cannot be related to polarization anisotropy of the emitted light as already observed for *a*-plane InAlN layers,[30] because a weak signal is always measured whatever the light polarization direction. The light emission properties of those MQWs are probably degraded by the poor surface quality generally obtained for nonpolar GaN substrates. Alternatively, this weak intensity may also be due to the presence of the cracks observed by TEM along the *c*-direction. A way to limit the formation of cracks would consist in minimizing the strain component by tuning the In content in $In_xAl_{1-x}N$ layers. The In content minimizing the elastic energy per volume unit E can be calculated from elasticity theory by

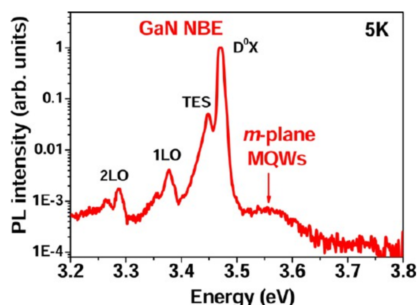

Figure 5. Photoluminescence spectrum of planar GaN/InAlN MQWs grown on *m*-GaN substrates measured at 5 K showing a weak emission of MQWs.

$$E = \frac{1}{2}\sum C_{ij}\varepsilon_i\varepsilon_j = \frac{1}{2}(2C_{12}\varepsilon_1\varepsilon_2 + C_{11}(\varepsilon_1^2 + \varepsilon_2^2) + \varepsilon_3(2C_{13}(\varepsilon_1 + \varepsilon_2) + C_{33}\varepsilon_3)) \quad (5)$$

where C_{ij} are the elastic constants and ε_i and ε_j are the strain values of the InAlN layer (i and j = 1−3). A value of x = 23% is obtained from this calculation, which is somewhat larger than the In content of our samples. However, the band offset in such In-rich GaN/InAlN MQWs would not necessarily guarantee the occurrence of an effective type-I QW band profile.

To limit the formation of structural defects, we propose an alternative approach using the sidewalls of *c*-oriented GaN wires acting as an *m*-plane template to grow GaN/InAlN MQWs. In this case, similar to the growth of InGaN/GaN MQWs,[13] we observe that the radial MQW growth occurs properly in the upper part of the GaN wires. Longitudinal and transversal cross-section STEM-HAADF images of a typical GaN wire coated by GaN/InAlN MQWs are shown in Figure 6a and b, respectively. *M*-plane growth of MQWs with the core-shell geometry is clearly observed with sharp interfaces along the sidewall facets of GaN wires (the bright regions correspond to GaN layers and the dark ones to InAlN layers). The thicknesses are equal to 2.1 nm for GaN wells and 4.6 nm for InAlN barriers, respectively (error bar about 0.1 nm), whatever the *m*-plane facets of the wires. These thicknesses are slightly smaller than those reported for *m*-plane planar growth but reveal a similar growth rate in both cases. A weak thickness

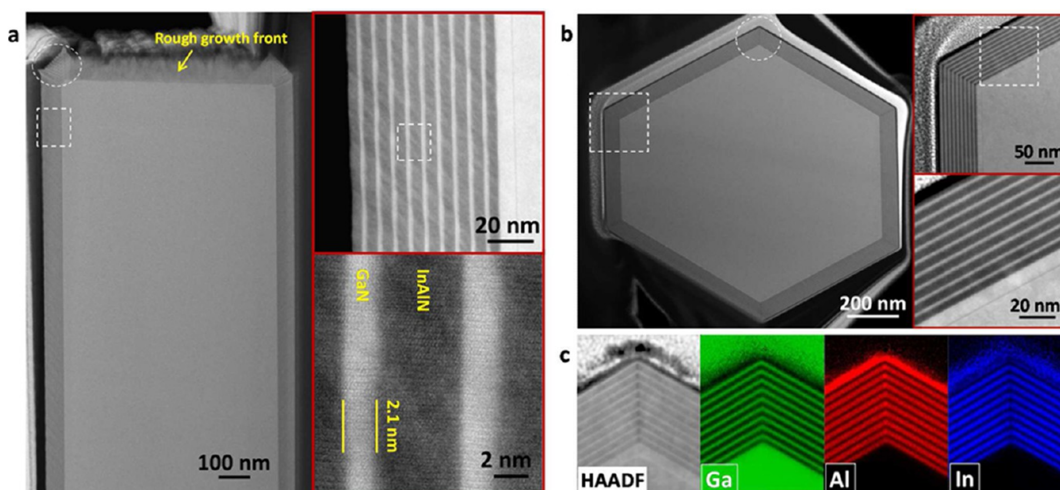

Figure 6. Cross-sectional TEM images of GaN wires with core−shell GaN/InAlN MQWs prepared by FIB: (a) longitudinal cross-sectional view taken along the [11−20] zone-axis with MQWs on the wire sidewalls and rough growth on the top wire facet (inset: enlarged view of the MQW region); (b) transversal cross-sectional view taken along the [0001] zone axis evidencing core−shell MQWs on *m*-plane hexagonal facets; (c) EDX chemical characterizations showing a HAADF image and the corresponding Ga, Al, and In mappings in green, red, and blue, respectively. An Al-rich region is clearly observed at the hexagon edges for InAlN barriers, which coincides with a convex shape, as emphasized in the longitudinal and transversal cross-section views (see white dashed circles).

gradient is observed along the wire length, corresponding to a reduction of about 3% per micrometer of the well and barrier thicknesses in the direction of the wire foot. In Figure 6a, a rough growth is noticeably observed on the *c*-plane top facet of GaN wires. We attribute this perturbed growth to the N-polar character of the *c*-plane flat top surface previously measured on such GaN wires in ref 33, because this phenomenon is not observed for the GaN/InAlN MQW growth on the current Ga-polar surface.[26] Further investigations on N-polar growths of InAlN would be required to confirm the impact of crystal polarity. In the longitudinal cross-section image taken along the [11−20] zone-axis shown in Figure 6a, no stacking fault is observed in the MQWs on the wire sidewalls, contrary to the case of InGaN/GaN MQWs published in ref 13. Interestingly, we do not observe the formation of cracks along the *c*-direction on longitudinal cross-section images (Figure 6a) contrary to planar growths. The defect-free character of such core−shell wires is attributed to the bounded size of the sidewall facets and of the edges (side hexagon length less than 500 nm) and also to the limited wire length, which can contribute to accumulate the *c*-axis strain. Also, the surface state of the wire sidewalls in terms of roughness, residual contamination and structural quality is certainly better than the usual planar *m*-plane surface, which may also contribute to limit the formation of defects. Figure 6c shows Ga, Al, and In chemical mappings measured by EDX. We clearly observe the core/shell GaN/InAlN MQW structure composed by GaN wells and InAlN barrier layers with sharp interface compositions. The InAlN barriers present homogeneous Al and In compositions, except at the wire edges where an Al enrichment is observed. The In content in InAlN is estimated by EDX to 15% (±2%) for the barriers grown on *m*-plane facets (i.e., same composition as for the planar structures), whereas only 7% (±2%) is extracted for the hexagon edges. This Al-rich composition is also observed in the HAADF-STEM images with a dark line visible in InAlN layers exactly at the edges of the hexagon (Figure 6c). The same Al-rich composition is measured on each of the six edges of the hexagonal wire section and also in the pyramidal shape of the MQWs grown in the lateral part on the top flat *c*-plane facet of the wire (circled parts in Figure 6a,b). Such a phenomenon has been already observed in core−shell AlP/InAlP[43] and AlGaAs/GaAs[44] heterostructures grown on GaAs nanowires. It has been explained by a shorter diffusion length of Al adatoms and a variation in the chemical potential with surface curvature.[45] These observations are also consistent with the In-poor regions observed for convex surface shapes on thick InAlN layers.[46]

The optical properties of wires dispersed on a Si substrate were characterized both by PL and CL measurements at 5 K. Figure 7a shows a typical low temperature PL spectrum of a dispersed core−shell wire assembly (red curve) and that of planar *c*-plane GaN/InAlN MQWs grown on a GaN template (black curve) that have the same GaN well thickness (i.e., 2.1 nm). Both spectra clearly exhibit two significant contributions: a main peak centered near 3.5 eV assigned to the NBE emission of bulk GaN and a second peak on the high-energy side ascribed to MQW emission. A red-shift of 160 meV attributed to the QCSE is clearly observed for the MQW emission in the case of polar *c*-plane growth with respect to the *m*-plane one. An emission energy equal to 3.584 eV is derived from envelope function calculations following a plane-wave expansion method (relying on the $k{\cdot}p$ method) and assuming a built-in electric field equal to 2 MV/cm[47] for the *c*-plane MQW growth. This result is very close to the experimental data since a MQW

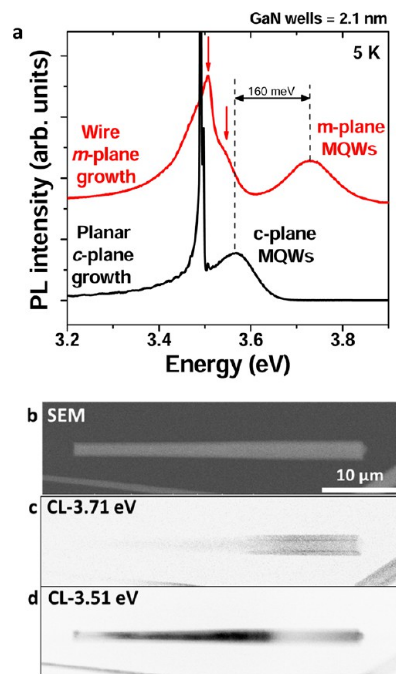

Figure 7. (a) Photoluminescence spectrum measured at 5 K of core−shell GaN/InAlN MQW dispersed wires (red curve) and that of planar *c*-plane GaN/InAlN MQWs grown on a GaN template (black curve) that have the same GaN well thickness (i.e., 2.1 nm). See text for details. (b−d) Cathodoluminescence analyses of single core−shell wires measured at 5 K showing a SEM image and the corresponding emission mappings measured at 3.51 and 3.71 eV, respectively.

emission peak at 3.57 eV is measured for the planar geometry. It also demonstrates the absence of QCSE for *m*-plane core-shell heterostructures, as expected for such nonpolar orientation, because in this latter case, the MQW peak emission is observed at ∼3.73 eV. The CL-mappings performed on single-wires confirm the peak origin, because the emission at 3.73 eV comes from the upper part of the wire covered by the radial GaN/InAlN MQWs (Figure 7c), whereas the GaN emission is mainly located on the bottom part (Figure 7d). The blueshift emission energy of those MQWs compared to the planar *m*-plane MQWs in the Figure 5 is mainly attributed to a larger quantum confinement because of the thinner GaN well thickness grown around the wire versus the planar structure one (2.1 vs 2.8 nm), in agreement with the simulation of energy dependence versus well thickness presented in the Figure 8e. Qian et al. reported an emission around 3.65−3.44 eV (340−360 nm) for radial AlN/GaN MQWs grown on triangular catalyzed GaN nanowires ascribed to both quantum confinement and strain effect.[17] In our case, we mainly attribute the emission energy to a higher confinement on nonpolar surfaces that improves the emission efficiency and avoids the critical red-shift usually observed in polar structures related to QCSE. In addition, a careful observation of the NBE emission in the PL spectrum shows the convolution of two emission lines. The dominant peak at 3.50 eV corresponds to the emission of unintentionally doped GaN located in the upper part of the wires and a shoulder at 3.56 eV is related to the *n*-doped part in the bottom of GaN wires due to Si doping and band-filling effect (Burstein-Moss shift), as previously depicted in ref 32.

Figure 8a shows temperature-dependent micro-PL measurements acquired at the tip of a single dispersed nanowire without polarization selection. In agreement with the previously

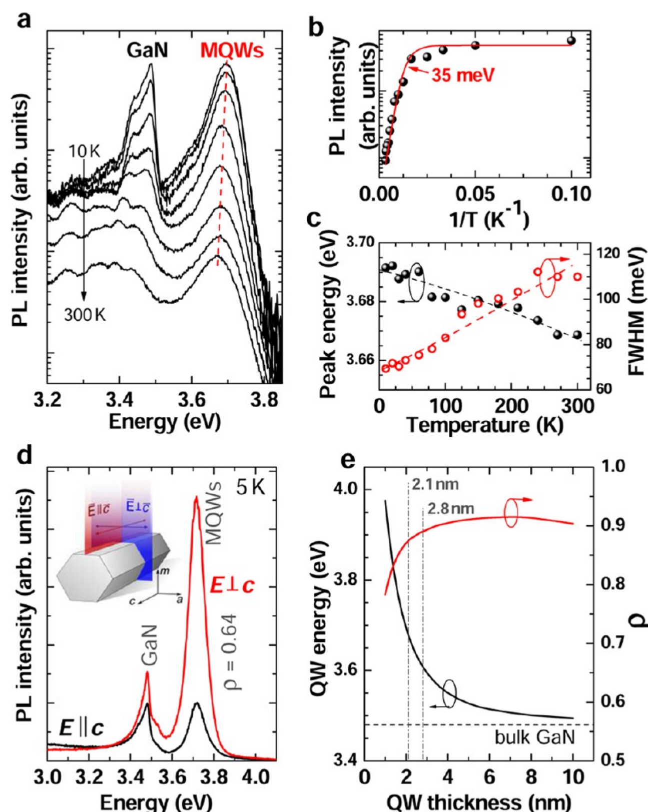

Figure 8. Microphotoluminescence measured on single core−shell wires. (a) Typical PL spectrum evolution as a function of temperature from 10 to 300 K. (b) Temperature-dependence of the MQW peak area revealing an activation energy of 35 meV. (c) Energy position and fwhm of the MQW emission peak as a function of temperature. (d) Low- temperature polarization-resolved PL spectra revealing anisotropic light emission. A significant polarization of the electric field vector perpendicular to the wire-axis is measured (ρ = 64%). (e) Simulated data using the $k{\cdot}p$ method to predict the energy position and the polarization of the emission of GaN/InAlN quantum wells grown on the m-plane as a function of QW thickness.

discussed PL and CL results, the spectra are dominated by two main contributions, namely, the MQW signal centered around 3.7 eV and the GaN NBE luminescence around 3.5 eV. The latter is strongly modulated, likely by optical modes present in the nanowires, which leads to an oscillatory behavior.[48,49] The MQW emission exhibits a low temperature inhomogeneous line width of ∼70 meV (cf. Figure 8c), which increases up to 110 meV at 300 K and competes with values measured on comparable high-quality polar GaN/InAlN structures.[26] The intensity ratio between room and low temperature is around 2%, which is comparable with the ratio reported for planar c-plane GaN/InAlN MQWs.[20] Taking into account the small emission energy shift with increasing temperature (20 meV), a dominating impact of carrier localization up to room temperature is expected, most probably due to interface fluctuations and In fluctuations present in the barriers. This interpretation fits well with the activation energy of 35 meV determined from the Arrhenius plot of the MQW PL integrated intensity shown in Figure 8b. A similar value has already been reported in polar InGaN/GaN QWs,[50] which was shown to be consistent with an activation energy ascribed to carrier delocalization from the potential minima rather than with thermal escape of the carriers from the confinement potential. Indeed, the latter process is unlikely owing to the large band offsets in the present QW system (e.g., >600 meV for the conduction band offset assuming a standard conduction to valence band offset ratio of 70:30). Note here that 35 meV may just be seen as a lower limit for the carrier localization energy when considering the low temperature emission line width. Calculations following the $k{\cdot}p$ method were performed in order to determine the QW transition energy as a function of the well width.[51] Appropriate band parameters and bandgaps were taken from ref 52, while the binding energy of 2D excitons was deduced from the method depicted in ref 53. The corresponding results are shown in Figure 8e. As expected for nonpolar GaN QWs free from built-in electric field, the transition energy converges toward the bulk GaN bandgap for large well widths. For the experimentally determined thickness of 2.1 nm, a low temperature transition energy of 3.68 eV is derived from this model. The difference with the experimentally observed low-temperature emission line centered at 3.695 eV might originate from different factors. First, the parameters from ref 52, including those governing the anisotropic effective valence band masses, are predominantly based on first-principles calculations and thus might potentially deviate from the real ones. On the other hand, the QW thickness slightly varies (3% per micrometer), leading to a total thickness variation ±0.3 nm, depending on the spot position along the wire axis.[13]

Simulations can also provide substantial information helping us to understand the behavior of the wires, for example, about the symmetry of the electronic states and thus about their polarization-dependent emission properties. In Figure 8d, low-temperature polarization-resolved PL spectra recorded on a single wire reveal several peculiarities. First, a significant anisotropy in the emission is visible for both the bulk GaN and the MQW signal as expected for nonpolar structures. Both emissions are copolarized, meaning that the highest emission intensity is found for a polarization of the electric field vector perpendicular to the optical axis, that is, to the wire axis. Although both emission lines are issued from GaN states, their similar behavior might be purely fortuitous. Indeed, the combination of quantum confinement and the experienced lattice strain is expected to influence the symmetry of the lowest energy level of the GaN QW. Figure 8e shows the evolution of the computed linear polarization degree ρ as a function of QW width. For the present QWs, a very high value, $\rho > 0.8$, is expected with a slightly decreasing value for thinner wells. Despite a qualitative agreement between the experimental finding and the simulations, the absolute experimental ρ value is lower ($\rho = 0.64$). All those simulations are only valid for free excitonic states. In view of the strong carrier localization, we could expect some deviations induced by a change in the symmetry of the confined states. Moreover, as the spot size amounts to ∼5 μm in this latter experiment, one can expect to collect not only the light issued from the well facet perpendicular to the incoming beam, but also from the 60° tilted side facets or scattered light from the wire tip (cf., Figure 6), which will exhibit a modified optical response. The same argumentation applies for the GaN NBE emission, where a reduced linear polarization degree with respect to the strain-free value is also observed.[54] Here, the impact of the degenerate conduction band from the n-doped region might additionally come into play.

In summary, we demonstrated the growth of nonpolar InAlN-based MQWs on m-plane surfaces either directly on m-GaN substrates or on the sidewalls of c-oriented GaN wires.

Although a perfect lattice matching cannot be reached for GaN/InAlN heterostructures on *m*-plane surfaces, pseudomorphic growth without dislocation or stacking fault has notably been established for planar GaN/InAlN MQWs with an In composition equal to 15%. A significant amount of strain occurring along the *c*-direction predicted by elasticity theory generates cracks along this direction. On the contrary, such cracks are not observed for core−shell growth on GaN wire sidewalls certainly due to stress relaxation of the wire facet free surfaces and edges. In contrast to planar growths, a strong luminescence occurring around 3.7 eV is observed in core/shell wires up to room temperature, which is attributed to the defect-free nature of MQWs. Based on those results and the recent demonstration of *p*-type InAlN,[55] the opportunity to develop InAlN-based UV light emitters that would benefit from wire sidewalls to grow high quality InAlN/GaN MQWs becomes realistic.

■ AUTHOR INFORMATION

Corresponding Author

*E-mail: christophe.durand@cea.fr.

Notes

The authors declare no competing financial interest.

■ ACKNOWLEDGMENTS

The authors thank J. Dussaud for technical MOCVD support, M. Terrier for the FIB sample preparation, Fabrice Donatini for CL guidance, and B. Gayral for fruitful discussions. Le Si Dang is also acknowledged for his help to build this project. C. Durand acknowledges financial support from the “pôle SMINGUE-FMN (Fédération Matière et Nanosciences)”, the program Franco-Swiss “Partenariats Hubert Curien (PHC) Germaine de Staël” and the French state funds ANR-10-LABX-51-01 (Labex LANEF du Programme d'Investissements d’Avenir).

■ REFERENCES

(1) Thelander, C.; Agarwal, P.; Brongersma, S.; Eymery, J.; Feiner, L. F.; Forchel, A.; Scheffler, M.; Riess, W.; Ohlsson, B. J.; Gösele, U.; et al. Nanowire-Based One-Dimensional Electronics. *Mater. Today* **2006**, *9*, 28−35.

(2) Pauzauskie, P. J.; Yang, P. Nanowire Photonics. *Mater. Today* **2006**, *9*, 36−45.

(3) Borgström, M. T.; Immink, G.; Ketelaars, B.; Algra, R.; Bakkers, E. P. A. M. Synergetic Nanowire Growth. *Nat. Nanotechnol.* **2007**, *2*, 541−544.

(4) Wallentin, J.; Anttu, N.; Asoli, D.; Huffman, M.; Aberg, I.; Magnusson, M. H.; Siefer, G.; Fuss-Kailuweit, P.; Dimroth, F.; Witzigmann, B.; et al. InP Nanowire Array Solar Cells Achieving 13.8% Efficiency by Exceeding the Ray Optics Limit. *Science* **2013**, *339*, 1057−1060.

(5) Björk, M. T.; Ohlsson, B. J.; Sass, T.; Persson, A. I.; Thelander, C.; Magnusson, M. H.; Deppert, K.; Wallenberg, L. R.; Samuelson, L. One-Dimensional Heterostructures in Semiconductor Nanowhiskers. *Appl. Phys. Lett.* **2002**, *80*, 1058−1060.

(6) Li, Y.; Xiang, J.; Qian, F.; Gradecak, S.; Wu, Y.; Yan, H.; Blom, D. A.; Lieber, C. M. Dopant-Free GaN/AlN/AlGaN Radial Nanowire Heterostructures as High Electron Mobility Transistors. *Nano Lett.* **2006**, *6*, 1468−1473.

(7) Qian, F.; Gradecak, S.; Li, Y.; Wen, C.-Y.; Lieber, C. M. Core/Multishell Nanowire Heterostructures as Multicolor, High-Efficiency Light-Emitting Diodes. *Nano Lett.* **2005**, *5*, 2287−2291.

(8) Qian, F.; Li, Y.; Gradecak, S.; Park, H.-G.; Dong, Y.; Ding, Y.; Wang, Z. L.; Lieber, C. M. Multi-Quantum-Well Nanowire Heterostructures for Wavelength-Controlled Lasers. *Nat. Mater.* **2008**, *7*, 701−706.

(9) Dong, Y.; Tian, B.; Kempa, T. J.; Lieber, C. M. Coaxial Group III-Nitride Nanowire Photovoltaics. *Nano Lett.* **2009**, *9*, 2183−2187.

(10) Li, S.; Waag, A. GaN Based Nanorods for Solid State Lighting. *J. Appl. Phys.* **2012**, *111*, 071101.

(11) Bavencove, A.; Salomon, D.; Lafossas, M.; Martin, B.; Dussaigne, A.; Levy, F.; André, B.; Ferret, P.; Durand, C.; Eymery, J.; et al. Light Emitting Diodes Based on GaN Core/Shell Wires Grown by MOVPE on N-Type Si Substrate. *Electron. Lett.* **2011**, *47*, 765−766.

(12) Choi, J. H.; Zoulkarneev, A.; Kim, S.; Baik, C. W., II; Yang, M. H.; Park, S. S.; Suh, H.; Kim, U. J.; Son, H. B.; Lee, J. S.; et al. Nearly Single-Crystalline GaN Light-Emitting Diodes on Amorphous Glass Substrates. *Nat. Photonics* **2011**, *5*, 763−769.

(13) Koester, R.; Hwang, J.; Salomon, D.; Chen, X.; Bougerol, C.; Barnes, J. P.; Dang, D. L.; Rigutti, L.; Bugallo, A. D. L.; et al. M-Plane Core-Shell InGaN/GaN Multiple-Quantum-Wells on GaN Wires for Electroluminescent Devices. *Nano Lett.* **2011**, *11*, 4839−4845.

(14) Kneissl, M.; Kolbe, T.; Chua, C.; Kueller, V.; Lobo, N.; Stellmach, J.; Knauer, A.; Rodriguez, H.; Einfeldt, S.; Yang, Z.; et al. Advances in Group III-Nitride-Based Deep UV Light-Emitting Diode Technology. *Semicond. Sci. Technol.* **2011**, *26*, 014036.

(15) Khan, A.; Balakrishnan, K.; Katona, T. Ultraviolet Light-Emitting Diodes Based on Group Three Nitrides. *Nat. Photonics* **2008**, *2*, 77−84.

(16) Taniyasu, Y.; Kasu, M.; Makimoto, T. An Aluminium Nitride Light-Emitting Diode with a Wavelength of 210 Nanometres. *Nature* **2006**, *441*, 325−328.

(17) Qian, F.; Brewster, M.; Lim, S. K.; Ling, Y.; Greene, C.; Laboutin, O.; Johnson, J. W.; Gradecak, S.; Cao, Y.; Li, Y. Controlled Synthesis of AlN/GaN Multiple Quantum Well Nanowire Structures and Their Optical Properties. *Nano Lett.* **2012**, *12*, 3344−3350.

(18) Lorenz, K.; Franco, N.; Alves, E.; Watson, I. M.; Martin, R. W.; O’Donnell, K. P. Anomalous Ion Channeling in AlInN/GaN Bilayers: Determination of the Strain State. *Phys. Rev. Lett.* **2006**, *97*, 085501.

(19) Butté, R.; Carlin, J.-F.; Feltin, E.; Gonschorek, M.; Nicolay, S.; Christmann, G.; Simeonov, D.; Castiglia, A.; Dorsaz, J.; Buehlmann, H. J.; et al. Current Status of AlInN Layers Lattice-Matched to GaN for Photonics and Electronics. *J. Phys. D: Appl. Phys.* **2007**, *40*, 6328−6344.

(20) Butté, R.; Cosendey, G.; Lugani, L.; Glauser, M.; Castiglia, A.; Perillat-Merceroz, G.; Carlin, J.-F.; Grandjean, N. In *III-Nitride Semiconductors and Their Modern Devices*; Gil, B., Ed.; Oxford University Press: Oxford, U.K., 2013.

(21) Gonschorek, M.; Carlin, J.-F.; Feltin, E.; Py, M. A.; Grandjean, N. High Electron Mobility Lattice-Matched AlInN/GaN Field-Effect Transistor Heterostructures. *Appl. Phys. Lett.* **2006**, *89*, 062106.

(22) Choi, S.; Kim, H. J.; Kim, S.-S.; Liu, J.; Kim, J.; Ryou, J.-H.; Dupuis, R. D.; Fischer, A. M.; Ponce, F. A. Improvement of Peak Quantum Efficiency and Efficiency Drop in III-Nitride Visible Light-Emitting Diodes with an InAlN Electron-Blocking Layer. *Appl. Phys. Lett.* **2010**, *96*, 221105.

(23) Carlin, J.-F.; Ilegems, M. High-Quality AlInN for High Index Contrast Bragg Mirrors Lattice Matched to GaN. *Appl. Phys. Lett.* **2003**, *83*, 668−670.

(24) Cosendey, G.; Castiglia, A.; Rossbach, G.; Carlin, J.-F.; Grandjean, N. Blue Monolithic AlInN-Based Vertical Cavity Surface Emitting Laser Diode on Free-Standing GaN Substrate. *Appl. Phys. Lett.* **2012**, *101*, 151113.

(25) Carlin, J.-F.; Zellweger, C.; Dorsaz, J.; Nicolay, S.; Christmann, G.; Feltin, E.; Butté, R.; Grandjean, N. Progresses in III-Nitride Distributed Bragg Reflectors and Microcavities Using AlInN/GaN Materials. *Phys. Status Solidi B* **2005**, *242*, 2326−2344.

(26) Nicolay, S.; Carlin, J.-F.; Feltin, E.; Butté, R.; Mosca, M.; Grandjean, N.; Ilegems, M. Midinfrared Intersubband Absorption in Lattice-Matched AlInN/GaN Multiple Quantum Wells. *Appl. Phys. Lett.* **2005**, *87*, 111106.

(27) Zhou, L.; Gonschorek, M.; Giraud, E.; Feltin, E.; Carlin, J.-F.; Grandjean, N.; Smith, D. J.; McCartney, M. R. Measurement of Polarization-Induced Electric Fields in GaN/AlInN Quantum Wells. *Appl. Phys. Lett.* **2012**, *101*, 251902.
(28) Waltereit, P.; Brandt, O.; Trampert, A.; Grahn, H.; Menniger, J.; Ramsteiner, M.; Reiche, M.; Ploog, K. Nitride Semiconductors Free of Electrostatic Fields for Efficient White Light-Emitting Diodes. *Nature* **2000**, *406*, 865−868.
(29) Rossbach, G.; Levrat, J.; Dussaigne, A.; Cosendey, G.; Glauser, M.; Cobet, M.; Butté, R.; Grandjean, N.; Teisseyre, H.; Bockowski, M.; et al. Tailoring the Light-Matter Coupling in Anisotropic Microcavities: Redistribution of Oscillator Strength in Strained *m*-Plane GaN/AlGaN Quantum Wells. *Phys. Rev. B* **2011**, *84*, 115315.
(30) Laskar, M. R.; Ganguli, T.; Rahman, A. A.; Arora, A.; Hatui, N.; Gokhale, M. R.; Ghosh, S.; Bhattacharya, A. Anisotropic Structural and Optical Properties of *a*-Plane (11−20) Nearly-Lattice-Matched to GaN. *Appl. Phys. Lett.* **2011**, *98*, 181108.
(31) Kajima, T.; Kobayashi, A.; Ueno, K.; Shimomoto, K.; Fujii, T.; Ohta, J.; Fujioka, H.; Oshima, M. Room-Temperature Epitaxial Growth of High-Quality *m*-Plane InAlN Films on Nearly Lattice-Matched ZnO Substrates. *Jpn. J. Appl. Phys.* **2010**, *49*, 070202.
(32) Koester, R.; Hwang, J. S.; Durand, C.; Dang, D. L. S.; Eymery, J. Self-Assembled Growth of Catalyst-Free GaN Wires by Metal-Organic Vapour Phase Epitaxy. *Nanotechnology* **2010**, *21*, 015602.
(33) Chen, X. J.; Perillat-Merceroz, G.; Sam-Giao, D.; Durand, C.; Eymery, J. Homoepitaxial Growth of Catalyst-Free GaN Wires on N-Polar Substrates. *Appl. Phys. Lett.* **2010**, *97*, 151909.
(34) Amstatt, B.; Landré, O.; Nicolin, V. F.; Proietti, M. G.; Bellet-Amalric, E.; Bougerol, C.; Renevier, H.; Daudin, B. Anisotropic Strain State of the [1−100] GaN Quantum Dots and Quantum Wires. *J. Appl. Phys.* **2008**, *104*, 063521.
(35) Hÿtch, M.; Snoeck, E.; Kilaas, R. Quantitative Measurement of Displacement and Strain Fields from HREM Micrographs. *Ultramicroscopy* **1998**, *74*, 131.
(36) Maruska, H. P.; Tietjen, J. J. The Preparation and Properties of Vapor-Deposited Single-Crystal-Line GaN. *Appl. Phys. Lett.* **1969**, *15*, 327.
(37) Moram, M. A.; Vickers, M. E. X-ray Diffraction of III-Nitrides. *Rep. Prog. Phys.* **2009**, *72*, 036502.
(38) Wright, A. F. Elastic Properties of Zinc-Blende and Wurtzite AlN, GaN, and InN. *J. Appl. Phys.* **1997**, *82*, 2833−2839.
(39) *Properties of Advanced Semiconductor Materials GaN, AlN, InN, BN, SiC, SiGe*; Levinshtein, M. E., Rumyantsev, S. L., Shur, M. S., Eds.; John Wiley & Sons, Inc.: New York, 2001.
(40) Lai, K. Y.; Paskova, T.; Wheeler, V. D.; Chung, T. Y.; Grenko, J. A.; Johnson, M. A. L.; Udwary, K.; Preble, E. A.; Evans, K. R. Indium Incorporation in InGaN/GaN Quantum Wells Grown on *m*-Plane GaN Substrate and *c*-Plane Sapphire. *Phys. Status Solidi A* **2012**, *209*, 559−564.
(41) Iso, K.; Yamada, H.; Hirasawa, H.; Fellows, N.; Saito, M.; Fujito, K.; DenBaars, S. P.; Speck, J. S.; Nakamura, S. High Brightness Blue InGaN/GaN Light Emitting Diode on Nonpolar *m*-Plane Bulk GaN Substrate. *Jpn. J. Appl. Phys.* **2007**, *46*, L960−962.
(42) Reshchikov, M. A.; Morkoç, H. Luminescence Properties of Defects in GaN. *J. Appl. Phys.* **2005**, *97*, 061301.
(43) Sköld, N.; Wagner, J. B.; Karlsson, G.; Hernán, T.; Seifert, W.; Pistol, M.-E.; Samuelson, L. Phase Segregation in AlInP Shells on GaAs Nanowires. *Nano Lett.* **2006**, *6*, 2743−2747.
(44) Heiss, M.; Fontana, Y.; Gustafsson, A.; Wüst, G.; Magen, C.; O'Regan, D. D.; Luo, J. W.; Ketterer, B.; Conesa-Boj, S.; Kuhlmann, A. V.; et al. Self-Assembled Quantum Dots in a Nanowire System for Quantum Photonics. *Nat. Mater.* **2013**, *12*, 439−444.
(45) Biasiol, G.; Kapon, E. Mechanisms of Self-Ordering of Quantum Nanostructures Grown on Nonplanar Surfaces. *Phys. Rev. Lett.* **1998**, *81*, 2962−2965.
(46) Perillat-Merceroz, G.; Cosendey, G.; Carlin, J.-F.; Butté, R.; Grandjean, N. Intrinsic Degradation Mechanism of Nearly Lattice-Matched InAlN Layers Grown on GaN Substrates. *J. Appl. Phys.* **2013**, *113*, 063506.
(47) The built-in electric field has been estimated to 3.6 MV/cm, as mentioned in ref 19 for the case of single quantum wells. For multiple quantum wells, the built-in field is reduced according to the geometrical effect inducing a redistribution of the field in the wells and the barriers (refs 56 and 57). It has been estimated to 2 MV/cm for the present MQW system.
(48) Coulon, P.-M.; Hugues, M.; Alloing, B.; Beraudo, E.; Leroux, M.; Zuniga-Perez, J. GaN Microwires as Optical Microcavities: Whispering Gallery Modes vs Fabry-Perot Modes. *Opt. Express.* **2012**, *20*, 18707−18716.
(49) Tessarek, C.; Sarau, G.; Kiometzis, M.; Christiansen, S. High Quality Factor Whispering Gallery Modes from Self-Assembled Hexagonal GaN Rods Grown by Metal-Organic Vapor Phase Epitaxy. *Opt. Express.* **2013**, *21*, 2733−2740.
(50) Cho, Y.-H.; Gainer, G. H.; Fischer, A. J.; Song, J. J.; Keller, S.; Mishra, U. K.; DenBaars, S. P. S-Shaped Temperature-Dependent Emission Shift and Carrier Dynamics in InGaN/GaN Multiple Quantum Wells. *Appl. Phys. Lett.* **1998**, *73*, 1370−1372.
(51) Scheibenzuber, W.; Schwarz, U. T.; Veprek, R. G.; Witzigmann, B.; Hangleiter, A. Calculation of Optical Eigenmodes and Gain in Semipolar and Nonpolar InGaN/GaN Laser Diodes. *Phys. Rev. B* **2009**, *80*, 115320.
(52) Vurgaftman, I.; Meyer, J. R. Band Parameters for Nitrogen-Containing Semiconductors. *J. Appl. Phys.* **2003**, *94*, 3675−3696.
(53) Leavitt, R. P.; Little, J. W. Simple Method for Calculating Exciton Binding Energies in Quantum-Confined Semiconductor Structures. *Phys. Rev. B* **1990**, *42*, 11774−11783.
(54) Misra, P.; Brandt, O.; Grahn, H. T.; Teisseyre, H.; Siekacz, M.; Skierbiszewski, C.; Łucznik, B. Complete In-Plane Polarization Anisotropy of the A Exciton in Unstrained *a*-Plane GaN Films. *Appl. Phys. Lett.* **2007**, *91*, 141903.
(55) Taniyasu, Y.; Carlin, J.-F.; Castiglia, A.; Butté, R.; Grandjean, N. Mg Doping for *p*-Type AlInN Lattice-Matched to GaN. *Appl. Phys. Lett.* **2012**, *101*, 082113.
(56) Bernardini, F.; Fiorentini, V. Spontaneous versus Piezoelectric Polarization in III-V Nitrides: Conceptual Aspects and Practical Consequences. *Phys. Status Solidi B* **1999**, *216*, 391−398.
(57) Grandjean, N.; Damilano, B.; Dalmasso, S.; Leroux, M.; Laügt, M.; Massies, J. Built-In Electric-Field Effects in Wurtzite AlGaN/GaN Quantum Wells. *J. Appl. Phys.* **1999**, *86*, 3714−3719.